Time-averaged transport in oscillatory squeeze flow of a viscoelastic fluid

Rui Yang,[1] Ivan C. Christov,[2] Ian M. Griffiths,[3] and Guy Z. Ramon[1,*]

[1]*Department of Civil and Environmental Engineering, Technion—Israel Institute of Technology, Haifa 32000, Israel*

[2]*School of Mechanical Engineering, Purdue University, West Lafayette, Indiana 47907, USA*

[3]*Mathematical Institute, University of Oxford, Radcliffe Observatory Quarter, Oxford OX2 6GG, United Kingdom*

(Received 27 May 2020; accepted 18 August 2020; published 15 September 2020)

Periodically driven flows are known to generate nonzero, time-averaged fluxes of heat or solute species, due to the interactions of out-of-phase velocity and temperature/concentration fields, respectively. Herein, we investigate such transport (a form of the well-known Taylor-Aris dispersion) in the gap between two parallel plates, one of which oscillates vertically, generating a time-periodic squeeze flow of either a Newtonian or a Maxwell fluid. Using the method of multiple time-scale homogenization, the mass/heat balance equation describing transport in this flow is reduced to a one-dimensional advection-diffusion-reaction equation. This result indicates three effective mechanisms in the mass/heat transfer in the system: an effective diffusion that spreads mass/heat along the concentration/temperature gradient, an effective advective flux, and an effective reaction that releases or absorbs mass/heat—in the time-averaged frame. Our results demonstrate that there exist resonant modes under which the velocity peaks when the dimensionless plate oscillation frequency (embodied by the Womersley number, the ratio of the transient inertia to viscous forces) approaches specific values. As a result, transport in this flow is significantly influenced by the dimensionless frequency. On the one hand, the effective, time-averaged dispersion coefficient is always larger than the molecular diffusivity and is sharply enhanced near resonance. The interaction between the fluid elasticity and the oscillatory forcing enhances the efficiency of transport in the system. On the other hand, the identified effective advection and reaction mechanisms may transport mass/heat from regions of high concentration/temperature to those of low concentration/temperature, or vice versa, depending on the value of the dimensionless frequency. Ultimately, it is shown that the oscillatory squeeze flow can either enhance or diminish transport, depending on the interplay of these three effective (homogenized) mechanisms.

DOI: 10.1103/PhysRevFluids.5.094501

I. INTRODUCTION

The spreading of a scalar in a flow due to the combined action of diffusion, advection, and reaction is widely known as Taylor-Aris (shear) dispersion [1–5]. Shear dispersion has been studied extensively, in particular, for flows that are oscillatory in time [6–11], due to their relevance to transport in arteries [12], in pulmonary airways [13–15], in cerebrospinal fluid [16], through bones [17], through liquid membranes [18] and wave boundary layers [19], through actuation via electro-osmotic forces [20,21], and so on. The analogous heat-transfer problem—generating a considerable

*ramong@technion.ac.il

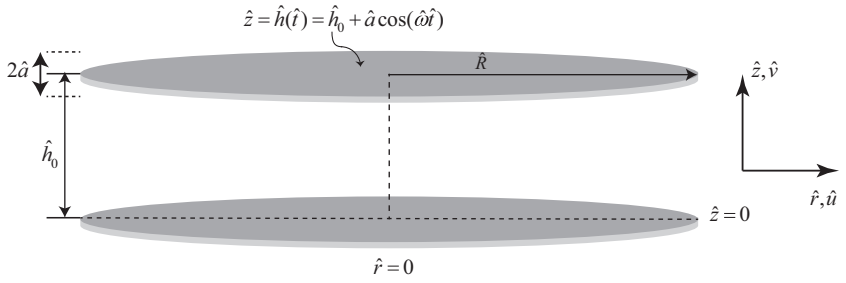

FIG. 1. Schematic of the oscillatory squeeze flow between two disks.

augmentation of the heat flux through flow oscillations—has also been observed (see, for example, [22–24]).

In what follows, we consider an oscillatory squeeze flow (OSF), in which a viscoelastic fluid is driven periodically by the motion of one of the confining, parallel planes (see Fig. 1 for a schematic of the studied configuration). This type of setting exists in some devices using magnetorheological fluids [25] or electrorheological fluids [26], where the fluid is squeezed periodically under a variable magnetic or electric field, as a means of achieving continuously variable control of mechanical vibrations, and is also envisioned as a mode of achieving control over transport in confined systems.

An early theoretical analysis of OSF was conducted by Phan-Thien and Tanner [27,28], who provided analytical solutions for the velocity profile and the normal force required to drive the plate. They proposed that the dynamic properties of polymeric liquids could be measured using a plastometer operating in the OSF mode. Since then, OSF equipment has been proposed and widely used in the rheology community for evaluating the processability of polymer melts, and for possible macromolecular characterization [29,30]. Furthermore, its ability to augment transport of mass and/or heat serves as a motivation for understanding the characteristics of this system.

Studies by Phan-Thien [27] and Bell *et al.* [31] demonstrated that a periodic flow in the streamwise direction (perpendicular to the oscillation direction of the plates) of an OSF exhibits a time dependence similar to that of an oscillatory pipe flow. Hence, there is reason to believe that shear-induced dispersion should also exist in the OSF, and dispersion would augment the mixing of the solute and the bulk flow along the streamwise direction. In this vein, Stone and Brenner [32] investigated the shear dispersion of a solute in a steady radial flow between two parallel plates and discovered a radially dependent effective diffusivity in the streamwise direction. Creech *et al.* [33] proposed a model to analyze dispersion in a specific case of the OSF, which occurs in the tear layer of the eye, sandwiched between the cornea and a soft contact lens. They found that the dispersion coefficient is orders of magnitude higher than the molecular diffusivity, facilitating mixing between the cornea and a soft contact lens. Specifically, the dispersion-augmented mixing is much faster than that which can be achieved by diffusion alone. However, the model neglects the advective contribution of streamwise velocity variations, while using a form of the velocity field valid for low frequencies. These simplifications limit the applicability of the study in Ref. [33]. In the present study, we relax these assumptions, while also extending it to the viscoelastic character of the fluid and its effect on Taylor-Aris dispersion.

In this paper, in view of the mathematical and physical analogy between mass diffusion and heat conduction, we investigate the dispersion in both contexts via a unified approach. We consider a domain confined by two parallel plates that enclose a Newtonian or a viscoelastic Maxwell fluid. One of the plates oscillates vertically in a sinusoidal fashion, squeezing the enclosed fluid. We determine the fluid velocity field and reduce the mass/heat balance equation to a one-dimensional advection-diffusion-reaction equation via the asymptotic method of multiple-scale homogenization. Interestingly, our results show that the OSF can either enhance or diminish mass/heat transfer, depending on the interplay of the effective diffusion, advection, and reaction mechanisms. To this

end, this paper is organized as follows: We begin by formulating the problem of the viscoelastic OSF between two plates. First, we obtain an analytical solution for the velocity profile in Sec. II A. Then, in Sec. II B, we combine the latter with the effective advection-diffusion-reaction equation for transport in the OSF. We present the results and discussion related to the velocity field in Sec. III A and the transport characteristics in Sec. III B. Concluding remarks are given in Sec. IV. Appendixes are included with a detailed derivation of the homogenized transport equation, as well as a calculation of the power required to drive the system.

II. MODEL FORMULATION

We consider the flow and scalar transport in a viscoelastic fluid confined between two concentric disks with the same radii, $\hat{R}$, separated by a distance $\hat{h}_0$ (see schematic in Fig. 1). The upper disk oscillates sinusoidally at amplitude $\hat{a}$ about a mean position $\hat{h}_0$, such that its position in time is $\hat{z} = \hat{h}(\hat{t})$, and the distance between the two disks is

$$\hat{h}(\hat{t}) = \hat{h}_0 + \hat{a}\cos(\hat{\omega}\hat{t}), \tag{1}$$

where $\hat{\omega}$ is the angular frequency, and $\hat{t}$ is the time. The vertical velocity of the top disk is therefore

$$\hat{h}'(\hat{t}) = -\hat{a}\hat{\omega}\sin(\hat{\omega}\hat{t}) = \mathrm{Re}\,\{\hat{a}\hat{\omega}ie^{i\hat{\omega}\hat{t}}\}, \tag{2}$$

where Re $\{\cdot\}$ denotes the real part of a complex quantity, and primes denote differentiation.

A. Velocity field

1. Governing equations

We begin with the equations of motion for an incompressible flow. The continuity equation is

$$\frac{1}{\hat{r}}\frac{\partial}{\partial\hat{r}}(\hat{r}\hat{u}) + \frac{\partial\hat{v}}{\partial\hat{z}} = 0, \tag{3}$$

where the two-dimensional velocity field is $\hat{\boldsymbol{u}} = \hat{u}\boldsymbol{e}_r + \hat{v}\boldsymbol{e}_z$, with $\boldsymbol{e}_r$ and $\boldsymbol{e}_z$ the unit vectors in the $\hat{r}$ and $\hat{z}$ directions, respectively (see Fig. 1), and the momentum equation, neglecting body forces, is

$$\hat{\rho}\frac{\mathrm{D}\hat{\boldsymbol{u}}}{\mathrm{D}\hat{t}} = -\nabla\hat{p} + \nabla\cdot\hat{\boldsymbol{\tau}}, \tag{4}$$

where $\hat{\boldsymbol{\tau}}$ is the (deviatoric) viscous stress tensor, $\hat{\rho}$ is the density of the fluid, and $\hat{p}$ is the pressure. The constitutive equation for the incompressible upper-convected Maxwell fluid (see, for example, [28]) is

$$\hat{\boldsymbol{\tau}} + \hat{\lambda}_0\left(\frac{\mathrm{D}\hat{\boldsymbol{\tau}}}{\mathrm{D}\hat{t}} - [\hat{\boldsymbol{\tau}}\cdot(\nabla\hat{\boldsymbol{u}}) + (\nabla\hat{\boldsymbol{u}})^T\cdot\hat{\boldsymbol{\tau}}]\right) = \hat{\mu}(\nabla\hat{\boldsymbol{u}} + \nabla\hat{\boldsymbol{u}}^T), \tag{5}$$

where $\hat{\lambda}_0$ is the viscoelastic relaxation time, and $\hat{\mu}$ is the usual, Newtonian, dynamic shear viscosity.

In what follows we assume that the amplitude of the disk oscillations is small, i.e., the dimensionless displacement amplitude of the upper plate $\delta = \hat{a}/\hat{h}_0 \ll 1$, while the frequency is unrestricted. With this assumption, combining Eq. (5) and Eq. (4) results in (see Appendix B for derivation)

$$\hat{\lambda}_0\frac{\partial^2\hat{u}}{\partial\hat{t}^2} + \frac{\hat{\lambda}_0}{\hat{\rho}}\frac{\partial^2\hat{p}}{\partial\hat{t}\partial\hat{r}} + \frac{\partial\hat{u}}{\partial\hat{t}} = -\frac{1}{\hat{\rho}}\frac{\partial\hat{p}}{\partial\hat{r}} + \frac{\hat{\mu}}{\hat{\rho}}\left(\frac{\partial^2\hat{u}}{\partial\hat{r}^2} + \frac{1}{\hat{r}}\frac{\partial\hat{u}}{\partial\hat{r}} + \frac{\partial^2\hat{u}}{\partial\hat{z}^2} - \frac{\hat{u}}{\hat{r}^2}\right), \tag{6a}$$

$$\hat{\lambda}_0\frac{\partial^2\hat{v}}{\partial\hat{t}^2} + \frac{\hat{\lambda}_0}{\hat{\rho}}\frac{\partial^2\hat{p}}{\partial\hat{t}\partial\hat{z}} + \frac{\partial\hat{v}}{\partial\hat{t}} = -\frac{1}{\hat{\rho}}\frac{\partial\hat{p}}{\partial\hat{z}} + \frac{\hat{\mu}}{\hat{\rho}}\left(\frac{\partial^2\hat{v}}{\partial\hat{r}^2} + \frac{1}{\hat{r}}\frac{\partial\hat{v}}{\partial\hat{r}} + \frac{\partial^2\hat{v}}{\partial\hat{z}^2}\right). \tag{6b}$$

We impose no slip and no penetration at the solid walls, which correspond to

$$\hat{u}(0) = 0, \quad \hat{u}(\hat{h}) = 0, \quad \hat{v}(\hat{h}) = \mathrm{Re}\,\{\hat{a}\hat{\omega}ie^{i\hat{\omega}\hat{t}}\}, \quad \hat{v}(0) = 0. \tag{7}$$

In principle, we must also specify conditions at $\hat{r} = \hat{R}$ to close the problem. We discuss this in more detail in Sec. II A 3.

2. Nondimensionalization

We posit lubrication-type scalings with the pressure made dimensionless using the viscous stress scale:

$$\hat{u} = \hat{U}u, \quad \hat{v} = \epsilon\hat{U}v, \quad \hat{t} = \hat{T}t, \quad \hat{r} = \hat{R}r, \quad \hat{z} = \epsilon\hat{R}z, \quad \hat{p} = \frac{\hat{\mu}\hat{U}}{\epsilon^2\hat{R}}p, \quad \hat{h} = \hat{h}_0 h. \tag{8}$$

Here, $\epsilon = \hat{h}_0/\hat{R}$. The vertical velocity scale $\epsilon\hat{U}$ is set by the oscillations of the wall, hence we have $\hat{U} = \hat{a}\hat{\omega}/\epsilon$. The natural time scale of the problem is the inverse of the oscillation frequency of the wall, i.e., $\hat{T} = 1/\hat{\omega}$. The dimensionless versions of the momentum equations (6a) and (6b) are then

$$\mathrm{De}\,\alpha^2\frac{\partial^2 u}{\partial t^2} + \mathrm{De}\frac{\partial^2 p}{\partial t\partial r} + \alpha^2\frac{\partial u}{\partial t} = -\frac{\partial p}{\partial r} + \epsilon^2\frac{\partial^2 u}{\partial r^2} + \epsilon^2\frac{1}{r}\frac{\partial u}{\partial r} + \frac{\partial^2 u}{\partial z^2} - \epsilon^2\frac{u}{r^2}, \tag{9a}$$

$$\epsilon^2\mathrm{De}\,\alpha^2\frac{\partial^2 v}{\partial t^2} + \mathrm{De}\frac{\partial^2 p}{\partial t\partial z} + \epsilon^2\alpha^2\frac{\partial v}{\partial t} = -\frac{\partial p}{\partial z} + \epsilon^2\left(\epsilon^2\frac{\partial^2 v}{\partial r^2} + \epsilon^2\frac{1}{r}\frac{\partial v}{\partial r} + \frac{\partial^2 v}{\partial z^2}\right), \tag{9b}$$

while the dimensionless form of the boundary conditions, (7), is

$$u(0) = 0, \quad u(1) = 0, \quad v(1) = \mathrm{Re}\,\{ie^{it}\}, \quad v(0) = 0. \tag{10}$$

Here, we define the Womersley number [34], $\alpha^2 = \hat{\rho}\hat{\omega}\hat{h}_0^2/\hat{\mu}$, the ratio of transient inertial forces to viscous forces, and the Deborah number, $\mathrm{De} = \hat{\lambda}_0\hat{\omega}$, the ratio of the elastic relaxation time scale to the oscillation time scale.

Combining Eqs. (9a) and (9b) at leading order in ϵ, we obtain

$$\mathrm{De}\,\alpha^2\frac{\partial^3 u}{\partial t^2\partial z} + \alpha^2\frac{\partial^2 u}{\partial t\partial z} = \frac{\partial^3 u}{\partial z^3}. \tag{11}$$

3. Solution

Assuming the form of the solutions

$$u(r, z, t) = \mathrm{Re}\left\{\frac{r}{2}f'(z)e^{it}\right\}, \tag{12a}$$

$$v(z, t) = -\mathrm{Re}\,\{f(z)e^{it}\} \tag{12b}$$

and substituting them into Eq. (11), we find that f satisfies the ordinary differential equation

$$(i - \mathrm{De})\alpha^2 f''(z) - f^{(4)}(z) = 0 \tag{13}$$

subject to the boundary conditions from Eq. (10):

$$f'(0) = 0, \quad f'(1) = 0, \quad f(1) = -i, \quad f(0) = 0. \tag{14}$$

We note that the solution structure, Eqs. (12a) and (12b), imposes a particular behavior of the fluid at $r = 1$. In practice one should apply appropriate conditions, which specify, for example, how the free surface moves or conditions on a reservoir into which the fluid enters beyond $r = 1$. However, these edge effects will play a small role in the overall behavior as a result of the lubrication approximation that we have made along with the assumption of small wall oscillations, and thus Eqs. (12a) and (12b) provides a suitable representation of the fluid flow.

The solution to Eq. (13) subject to (14) is

$$f(z) = -\frac{ie^{\Gamma(1-z)}(e^{\Gamma(z-1)}(\Gamma z - e^{\Gamma z} + e^{\Gamma}(\Gamma z - 1) + 1) + 1)}{e^{\Gamma}(\Gamma - 2) + \Gamma + 2}, \tag{15}$$

where $\Gamma = \alpha\sqrt{i - \mathrm{De}}$. Thus, the dimensionless velocity components are

$$u(r, z, t) = -\mathrm{Re}\left\{\frac{r}{2}e^{it}\frac{i\Gamma(e^{\Gamma} - e^{\Gamma z} - e^{\Gamma - \Gamma z} + 1)}{e^{\Gamma}(\Gamma - 2) + \Gamma + 2}\right\}, \tag{16a}$$

$$v(z, t) = \mathrm{Re}\left\{\frac{ie^{\Gamma(1-z)}(e^{\Gamma(z-1)}(\Gamma z - e^{\Gamma z} + e^{\Gamma}(\Gamma z - 1) + 1) + 1)}{e^{\Gamma}(\Gamma - 2) + \Gamma + 2}e^{it}\right\}. \tag{16b}$$

B. Time-averaged scalar dispersion: Mass and heat transfer

1. Governing equations

For the flow sketched in Fig. 1 given by the solution in Eqs. (16a) and (16b), the advection-diffusion equation governing the mass and heat transfer (in the absence of mass/heat sources or sinks) can be expressed as

$$\frac{\partial\hat{\Lambda}}{\partial\hat{t}} + \left(\frac{1}{\hat{r}}\frac{\partial(\hat{r}\hat{u}\hat{\Lambda})}{\partial\hat{r}} + \frac{\partial(\hat{v}\hat{\Lambda})}{\partial\hat{z}}\right) = \hat{D}\frac{1}{\hat{r}}\frac{\partial}{\partial\hat{r}}\left(\hat{r}\frac{\partial\hat{\Lambda}}{\partial\hat{r}}\right) + \hat{D}\frac{\partial^2\hat{\Lambda}}{\partial\hat{z}^2}, \tag{17}$$

where $\hat{D}$ is the mass or thermal diffusivity, and $\hat{\Lambda}$ represents either the concentration or the temperature for the cases of mass and heat transfer, respectively. Note that, for the equivalence between mass and heat transfer to hold, we assume that the viscous dissipation in heat transfer is negligible. This assumption is valid when the Brinkman number is small, i.e., $\sigma\hat{U}^2/(\hat{\Lambda}_{\max} - \hat{\Lambda}_{\min})\hat{c}_p = \mathrm{o}(\epsilon^2)$, where $\hat{\Lambda}_{\max}$, $\hat{\Lambda}_{\min}$, and $\hat{c}_p$ represent the maximum temperature, minimum temperature, and specific heat capacity, respectively. The walls of the plates are impermeable and thermally insulated, thus we have the following boundary conditions:

$$\left.\frac{\partial\hat{\Lambda}}{\partial\hat{z}}\right|_{\hat{z}=0} = \left.\frac{\partial\hat{\Lambda}}{\partial\hat{z}}\right|_{\hat{z}=\hat{h}(\hat{t})} = 0. \tag{18}$$

To close the problem we also require boundary conditions at a fixed radial position, however, these are not necessary to determine the radially averaged governing equation; we consider a particular case in Sec. III B 2.

By introducing the dimensionless variables from Eq. (8) and the dimensionless concentration/temperature $\Lambda = (\hat{\Lambda} - \hat{\Lambda}_{\min})/(\hat{\Lambda}_{\max} - \hat{\Lambda}_{\min})$, Eqs. (17) and (18) become

$$\alpha^2\sigma\frac{\partial\Lambda}{\partial t} + \epsilon\mathrm{Pe}\left(\frac{1}{r}\frac{\partial(ru\Lambda)}{\partial r} + \frac{\partial(v\Lambda)}{\partial z}\right) = \frac{\epsilon^2}{r}\frac{\partial}{\partial r}\left(r\frac{\partial\Lambda}{\partial r}\right) + \frac{\partial^2\Lambda}{\partial z^2}, \tag{19a}$$

$$\left.\frac{\partial\Lambda}{\partial z}\right|_{z=0} = \left.\frac{\partial\Lambda}{\partial z}\right|_{z=h} = 0, \tag{19b}$$

where $\mathrm{Pe} = \hat{h}_0\hat{U}/\hat{D}$ is the Péclet number and $\sigma = \hat{\mu}/\hat{\rho}\hat{D}$ is the Schmidt number in mass transfer or the Prandtl number in heat transfer.

2. Multiple-time-scale analysis

We now turn to the derivation of the time-averaged transport equation, for which we employ the technique of multiple-time-scale homogenization [35]. There are three disparate time scales in this problem; first, the characteristic time for mass/heat diffusion in the transverse direction is

$$\hat{t}_0 = O\left(\frac{\hat{h}_0^2}{\hat{D}}\right). \tag{20}$$

We assume that this time scale is comparable to the oscillation period, i.e., $\hat{t}_0 = O(1/\hat{\omega})$, which means that the mass/heat diffusion in the transverse direction should equilibrate within several

oscillation periods [36,37]. The second time scale is the characteristic time for advection in the streamwise direction:

$$\hat{t}_1 = \frac{\hat{t}_0}{\epsilon} = O\left(\frac{\hat{R}}{\hat{U}}\right). \tag{21}$$

The third, and longest, time scale is for streamwise diffusion:

$$\hat{t}_2 = \frac{\hat{t}_0}{\epsilon^2} = O\left(\frac{\hat{R}^2}{\hat{D}}\right). \tag{22}$$

In the multiple-time-scale analysis, we assume that all variables are dependent on these three time scales *independently* [35,38]. Then, using the dimensionless versions of these time scales, the time derivative transforms as

$$\frac{\partial}{\partial t} = \frac{\partial}{\partial t_0} + \frac{\mathrm{d}t_1}{\mathrm{d}t}\frac{\partial}{\partial t_1} + \frac{\mathrm{d}t_2}{\mathrm{d}t}\frac{\partial}{\partial t_2} = \frac{\partial}{\partial t_0} + \epsilon\frac{\partial}{\partial t_1} + \epsilon^2\frac{\partial}{\partial t_2}. \tag{23}$$

We follow Fife and Nicholes [39] and expand Λ as follows:

$$\Lambda \sim \Lambda_0(r, z, t_1, t_2) + \sum_{n=1}^{\infty} \epsilon^n \Lambda_n(r, z, t_0, t_1, t_2) + \sum_{n=0}^{\infty} \epsilon^n W_n(r, z, t_0), \tag{24}$$

where the Λ_n terms are assumed to be fully developed terms that are harmonic functions of t_0, while the W_n terms are assumed to be transient in t_0 and vanish as $t_0 \to \infty$.

Next, homogenization [36,40] is performed (see details in Appendix A), which transforms Eq. (19a) into a homogenized advection-diffusion-reaction equation for transport in the viscoelastic OSF,

$$\alpha^2\sigma\frac{\partial \Lambda_0}{\partial t_2} = \frac{1}{r}\frac{\partial}{\partial r}\left((1 + D_{\mathrm{eff}})r\frac{\partial \Lambda_0}{\partial r} - rU_{\mathrm{eff}}\Lambda_0\right) + S_{\mathrm{eff}}\Lambda_0, \tag{25}$$

where

$$D_{\mathrm{eff}}(r) = -\frac{r^2}{4}\mathrm{Pe}\,\mathrm{Re}\,\langle f'^{*}B_{\mathrm{w}}\rangle, \tag{26a}$$

$$U_{\mathrm{eff}}(r) = -\frac{r}{2}\mathrm{Pe}\,\mathrm{Re}\,\{iB_{\mathrm{w}}(1)\}, \tag{26b}$$

$$S_{\mathrm{eff}} = -\mathrm{Pe}\,\mathrm{Re}\,\{iB_{\mathrm{w}}(1)\}. \tag{26c}$$

Here, the superscript asterisk represents the conjugate of a complex number, and we have further defined

$$B_{\mathrm{w}}(z) = \frac{\Gamma\mathrm{Pe}\,e^{-z(\Gamma+2A_1)}[A_2(-e^{A_3} + e^{\Gamma+A_1(2z+1)+\Gamma z} + e^{A_1(2z+1)+\Gamma z} - e^{z(\Gamma+2A_1)}) + A_4]}{2\alpha^2\sigma A_2[e^{\Gamma}(\Gamma-2)+\Gamma+2](e^{A_1}-1)},$$

$$A_1 = (-1)^{1/4}\alpha\sqrt{\sigma},$$

$$A_2 = \alpha^2\sigma + i\Gamma^2,$$

$$A_3 = \Gamma + 2A_1 z + \Gamma z,$$

$$A_4 = iA_1^2(e^{\Gamma+2A_1z+A_1} + e^{2A_1z+A_1+2\Gamma z} - e^{2z(\Gamma+A_1)} - e^{\Gamma+2A_1z}) - iA_1\Gamma(e^{(z+1)(\Gamma+A_1)} - e^{A_1z+A_1+\Gamma z} + e^{\Gamma+3A_1z+\Gamma z} - e^{(\Gamma+3A_1)z}).$$

Using Eq. (23), t_2 in Eq. (25) can be replaced by the general time t, resulting in

$$\frac{\alpha^2\sigma}{\epsilon^2}\frac{\partial \Lambda_0}{\partial t} = \frac{1}{r}\frac{\partial}{\partial r}\left((1 + D_{\mathrm{eff}})r\frac{\partial \Lambda_0}{\partial r} - rU_{\mathrm{eff}}\Lambda_0\right) + S_{\mathrm{eff}}\Lambda_0. \tag{27}$$

Note that the above equation is valid on the long time scale, i.e., $t \gtrsim t_2$. By recalling $\hat{t}_0 \ll \hat{t}_1 \ll \hat{t}_2$ and substituting Eqs. (20) to (22) into this inequality, we obtain a restriction on the range of Pe, i.e., $\epsilon \ll \mathrm{Pe} \ll 1/\epsilon$, to ensure validity of our theory. Further, by substituting Eq. (20) into the assumption of $\hat{t}_0 = O(1/\hat{\omega})$, we obtain $\alpha^2\sigma = O(1)$.

Equation (27) is the homogenized effective advection-diffusion-reaction equation for transport in the viscoelastic OSF, which embodies three effective mechanisms of mass/heat transfer comprising the dispersion process. The first one is the effective diffusion, with D_{eff} representing the effective streamwise diffusivity. As with molecular diffusion (Fick's law), the effective diffusive flux is also driven by the concentration gradient. The second is the effective advection, which indicates that mass/heat is carried along by an effective streamwise advection velocity U_{eff}, representing a time-averaged drift velocity. When $U_{\mathrm{eff}} > 0$, it is directed radially outwards; when $U_{\mathrm{eff}} < 0$, it is directed radially inwards. The third mechanism of mass/heat transfer is an effective reaction term, releasing/absorbing solute or heat when $S_{\mathrm{eff}} > 0$ or $S_{\mathrm{eff}} < 0$, respectively. This reaction term arises as a result of the wall motion; we recall that no mass or heat is absorbed or emitted by the walls. The ratio $U_{\mathrm{eff}}/S_{\mathrm{eff}} = r/2$, indicating that the effect of effective advection is much less significant than effective reaction when $r \ll 1$, which is expected given the structure of the velocity field. When the effective advection and reaction work against the concentration/temperature gradient, and their effects on transport exceed that of effective diffusion, the spreading of mass/heat will be inhibited. This is similar to the finding of a negative time-averaged dispersion coefficient [41], with which the solute cloud will be compressed in the oscillatory flow. Additionally, these three effective mechanisms are not independent, as they all depend on the dimensions of the device, motion of the plate, and properties of the fluid.

Comparing Eq. (27) with the long-time equations obtained in similar treatments of transport in oscillatory pipe flow [20,36,37,41], we find that the dispersion process in an OSF is different, in two aspects. First, the effective advection and reaction terms occur, beyond the usual dispersion term; these appear due to the first-order term at the boundary, which is embodied in $B_w(1)$. Second, D_{eff} varies in the streamwise (i.e., radial) direction, as well as U_{eff}. The main reason is that the radial velocity component varies in the streamwise direction, which is also a feature of steady radial flow with converging and diverging streamlines [32].

III. RESULTS AND DISCUSSION

A. Velocity field

In Fig. 2, we present the profiles of the horizontal velocity u at different times at the fixed cross section $r = 1$. Note that the value of r is chosen arbitrarily for illustrative purposes; the shape of the velocity profile is unchanged by varying r. Comparing Figs. 2(a) and 2(c), we observe that the Newtonian fluid's velocity profile u becomes flatter near the centerline when α is relatively large. In this case, the forcing scale is smaller than the viscous time scale, so the effects of the oscillation of the top plate are confined to near the wall during one oscillation period, and the fluid in the centerline is not influenced. The negligible pressure gradient in the z direction for $\mathrm{De} = 0$ [see Eq. (9b)] ensures the profile in near centerline remains flat. However, when α is small, the oscillations are slow enough that viscosity affects the entire cross section, as shown in Fig. 2(a). The velocity profiles shown in Figs. 2(a) to 2(c) exhibit similar variations with α as the oscillatory flow in a pipe [20,42,43].

Next, comparing Figs. 2(d) and 2(f), we observe that the velocity has multiple local maxima, across the gap, when $\mathrm{De} \gg 1$. The Deborah number De is the ratio of the elastic relaxation time to the oscillation time scale of the OSF, which is set by the plate motion. For a Newtonian fluid ($\mathrm{De} = 0$), the flow generated by the movement of the plate is felt instantaneously throughout the entire gap. For a viscoelastic fluid ($\mathrm{De} > 0$), on the other hand, the elasticity of the fluid acts as a restoring force that inhibits the transfer of momentum from the oscillatory wall. Thus, for larger values of De, the influence of the motion of the plate lags behind the forcing, i.e., it takes "longer"

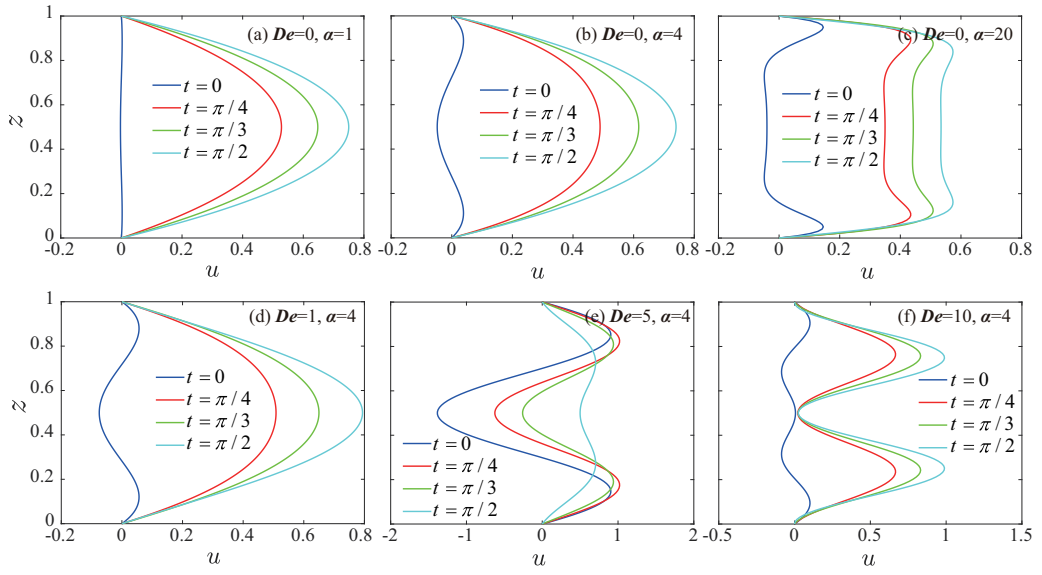

FIG. 2. Dimensionless streamwise velocity u variation across the gap height z at $r = 1$. Different values of De and α highlight the effects of viscoelasticity and oscillatory forcing.

to be felt throughout the domain. As a result, the fluid near the center lags behind the fluid near the wall, leading to the multiple peaks in the velocity distribution across the gap.

The nature of the fluid flow also changes dramatically at some specific values of De and α. For instance, the phase of u when $\mathrm{De} = 5$ and $\alpha = 4$ [Fig. 2(e)] is very different from the other cases shown. This is attributed to the triggering of a 'resonant' mode. To understand and quantify this effect, we introduce the spatiotemporal average of the longitudinal velocity

$$u_{\mathrm{a}}(r) = \frac{1}{2\pi}\int_0^1\int_0^{2\pi} |u(r, z, t)|\mathrm{d}t\mathrm{d}z. \tag{28}$$

The dependence of u_{a} on α for different values of De at radial position $r = 1$ is shown in Fig. 3. It can be seen that, for a viscoelastic fluid ($\mathrm{De} > 0$), there are peaks of u_{a} at specific values of α.

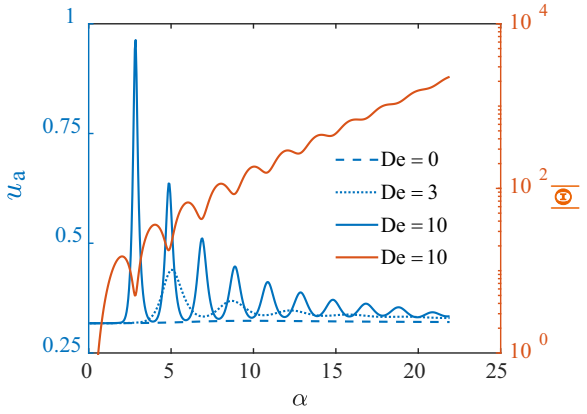

FIG. 3. The dependence of the spatiotemporal average of the r-direction velocity, u_{a} from Eq. (28), and the absolute value of the denominator of u, $|\Theta|$ from Eq. (30), on α at $r = 1$.

This phenomenon is caused by the elasticity of the fluid, hence we term it a *viscoelastic resonance*. The corresponding value of α can be considered the dimensionless resonant frequency. This effect has also been observed in the oscillatory pipe flow of a Maxwell fluid both experimentally [44] and numerically [24].

We find that the variation of u_a is mainly determined by the denominator of u, while its numerator is much less significant. We therefore introduce a parameter

$$\Theta(\alpha, \mathrm{De}) = e^{\Gamma}(\Gamma - 2) + \Gamma + 2, \tag{29}$$

representing the denominator of u. As shown in Fig. 3, the peaks of u_a coincide with the local minima of $|\Theta|$ when $\mathrm{De} = 10$. We further compared the match between the peaks of u_a and minima of $|\Theta|$ for $\mathrm{De} \leqslant 100$, observing that they match without exception for this range. Hence, it can be deduced that the resonance is governed by $|\Theta|$, which is a manifestation of the elasticity of the fluid. For a Maxwell fluid, as α increases, the amplitude of the oscillations of $|\Theta|$ decreases, while $|\Theta|$ continues to increase, leading to the decay of the oscillations. This effect can be interpreted as viscous forces overcoming the elastic restoring force. Consequently, the peaks of u_a gradually decrease with increasing α and eventually disappear beyond some critical value.

The resonant values of α satisfy $\partial|\Theta|/\partial\alpha = 0$, corresponding with local minima of $|\Theta|$. Specifically, beginning with Eq. (29) and aided by numerical experimentation, we find the following approximation for the α value corresponding to the nth peak,

$$\alpha_n^* \approx \frac{\pi(2n+1)}{\mathrm{Im}\{\sqrt{i - \mathrm{De}}\}}, \tag{30}$$

where $\mathrm{Im}\{\cdot\}$ denotes the imaginary part of a complex number, and $n \in \mathbb{N}^+$, such that the α corresponding to the first peak of u_a can be approximated with $n = 1$, the second peak with $n = 2$, and so on. Comparing the estimated values of α_n^* obtained from Eq. (30) and the corresponding exact values in the range of $\mathrm{De} \leqslant 100$ and $n \leqslant 10$, we find that the deviations are quite small and gradually decrease as De increases. For instance, the error in α_1^* is 0.32 (6.3%), 0.21 (5.4%), and 0.04 (4.7%) for $\mathrm{De} = 3$, $\mathrm{De} = 5$, and $\mathrm{De} = 100$, respectively.

Equation (30) also indicates that, as De is increased, the value of α_n^* decreases for fixed n, as does the interval between neighboring resonant peaks, as shown in Fig. 3. Note that there is no visible peak for a Newtonian fluid when the value of α reaches α_1^*, which is 13.33 according to Eq. (30), in Fig. 3, because the amplitude of fluctuation of $|\Theta|$ is too low to be compared with its absolute value. As De increases, the height of the peaks, especially the first peak, increases, presumably because for larger De, the value of α_1^* decreases (see Eq. (30)), thus $|\Theta|$ becomes very small, leading to a very high peak of u_a. This viscoelastic resonance is significant for the mass and heat transfer in the OSF, which is discussed in the following section.

B. Time-averaged transport characteristics

1. Effective dispersion, advection, and reaction

In this section, we first discuss how D_{eff}, U_{eff}, and S_{eff}, at the cross section of $r = 1$, vary with the Womersley α, Deborah De, and Schmidt (or Prandtl) σ numbers. As with the discussion of velocity field in Sec. III A, the value of r is chosen for illustrative purposes, and this choice does not affect the general characteristics identified. To facilitate the discussion, we introduce the tidal displacement, which represents the cross-sectionally averaged longitudinal distance traversed by a fluid particle under the OSF velocity field over half a period. This quantity is calculated through the spatiotemporal average of the velocity magnitude,

$$\Delta r(r) = \frac{\delta}{2\epsilon}\int_0^1\int_0^{2\pi} |u(r, z, t)|\,\mathrm{d}t\,\mathrm{d}z = \frac{\pi\delta}{\epsilon}u_a(r), \tag{31}$$

where u_a is defined by Eq. (28) and must be evaluated numerically.

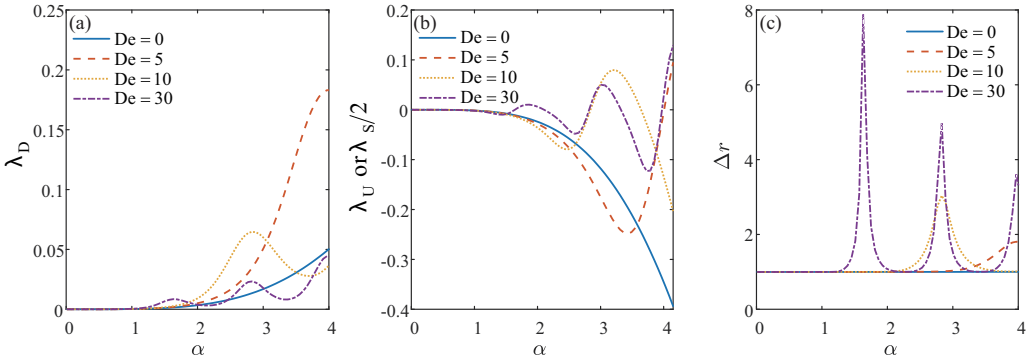

FIG. 4. The dependence of λ_D, λ_U (or $\lambda_S/2$), and Δr on α for different values of De, at $r = 1$ with $\sigma = 0.6$. Δr is obtained with $\delta = \epsilon$. The value of Pe is determined by $\mathrm{Pe} = \alpha^2\sigma\delta/\epsilon$. Note that $\lambda_U = \lambda_S/2$ for $r = 1$.

In addition, following Kurzweg and Jaeger [45], who scaled the effective diffusivity (the dispersion coefficient) for an oscillatory pipe flow by the product of the frequency and the square of the tidal displacement, we define the rescaled diffusivity, advection velocity, and reaction coefficients for the OSF:

$$\lambda_D = \frac{D_{\mathrm{eff}}}{\Delta r^2}, \quad \lambda_U = \frac{U_{\mathrm{eff}}}{\Delta r^2}, \quad \lambda_S = \frac{S_{\mathrm{eff}}}{\Delta r^2}. \tag{32}$$

After this rescaling, λ_D, λ_U, and λ_S are independent of the dimensionless displacement of the upper plate, i.e., δ. Since Δr depends on δ, λ_D, λ_U, and λ_S can also be independent of Δr if u_a and ϵ stay fixed according to Eq. (31).

It is important to note that λ_D, λ_U, and λ_S strongly depend on the values of α and De, as shown in Fig. 4. Specifically, optimal values of α have local maxima in terms of λ_D, which depend on the value of De. For a given range of α, increasing De will generate more peaks but not necessarily a higher value of λ_D. As an example, λ_D has a maximum at $\alpha = 4$, when $\mathrm{De} = 30$, but this maximum value is not higher than the one for $\mathrm{De} = 0$. For a Maxwell fluid ($\mathrm{De} > 0$), the maximum values of λ_D increase with α, in accordance with the oscillatory pipe flow in which the effective diffusivity is proportional to the frequency [45].

The peaks in Fig. 4(a) are the resonant values of λ_D, because the corresponding values of α appear to closely match the resonant frequencies, i.e., the values of α correspond to the peaks in Fig. 4(c). In other words, the resonance sharply increases the values of both λ_D and Δr. Hence, the locations of peaks in Figs. 4(a) and 4(c) can be approximated by Eq. (30), although with slight deviations. From Figs. 4(a) and 4(c), we observe opposite trends of the height of peaks in λ_D and Δr with increasing α. Accordingly, the value of D_{eff} might be dominated by Δr for a Maxwell fluid with a relatively large De at small α or, conversely, by λ_D for a weakly viscoselastic fluid (small De) but at a large α. For instance, when $\alpha = 1.64$ with $\mathrm{De} = 30$, the value of D_{eff} is two orders of magnitude larger than that with the absence of resonance, which is mainly attributed to Δr, which is increased by a factor of 8 by resonance.

The fact that the ratio $\lambda_U/\lambda_S = r/2$ indicates that transport due to the effective advection is much less significant than that due to effective reaction when $r \ll 1$. In Fig. 4(b), for a Newtonian fluid ($\mathrm{De} = 0$), λ_U and λ_S are negative, indicating that the effective advection is always directed from the edge of the plate towards the center, and the effective reaction absorbs mass/heat. For a Maxwell fluid, λ_U and λ_S fluctuate around 0, with the amplitude increasing with α, indicating that the effect of the effective advection and reaction, i.e., carrying mass/heat from a high-concentration region to a low-concentration region or along the opposite direction, is very sensitive to the oscillatory forcing of the system (quantified by α).

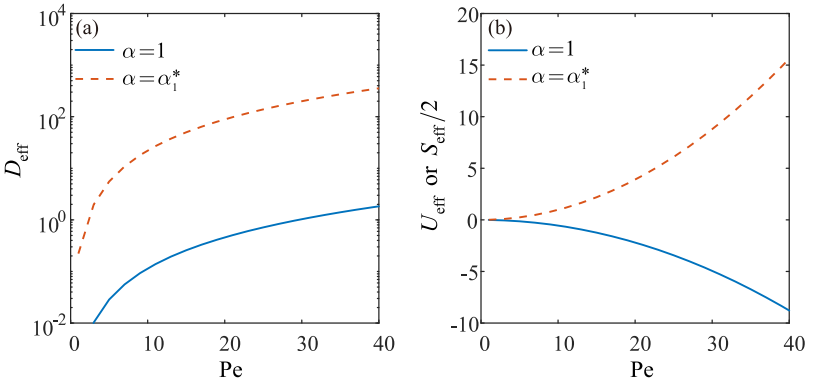

FIG. 5. The dependence of D_{eff} and U_{eff} (or $S_{\text{eff}}/2$) on Pe, at $r = 1$ when De $= 30$ and $\sigma = 3$. Two values of α are shown: $\alpha = 1$ (no resonance) and $\alpha_1^* = 1.64$ (first resonant mode). The value of α_1^* was obtained numerically. Note that $U_{\text{eff}} = S_{\text{eff}}/2$ for $r = 1$.

Figure 5 shows the dependence of D_{eff}, U_{eff}, and S_{eff} on Pe, at the first resonant mode, and with the absence of resonance. Importantly, D_{eff} is significantly increased by the existence of a viscoelastic resonance, because both Δr and λ_{D} reach the peak values according to Fig. 4. The strongest enhancement exists at the first resonant mode ($\alpha_1^* = 1.64$), where the value of D_{eff} is around 200 times larger than the corresponding value (at the same Pe) but in the absence of a resonance. Similarly, U_{eff} and S_{eff} also increase, although less significantly. Moreover, we can achieve larger D_{eff}, U_{eff}, and S_{eff} by increasing the displacement amplitude of the upper plate, which is captured by Pe.

It is important to note, however, that large values of D_{eff}, U_{eff}, and S_{eff} do not necessarily lead to the enhancement of mass/heat transfer: the transport in the OSF is controlled jointly by the interaction of these three effective (homogenized) transport mechanisms. The effective diffusion (dispersion) always enhances transport, but whether the effective advection or reaction enhances or impedes transport depends on whether they are directed along or against the concentration gradient, which is determined by the signs of λ_{U} (or U_{eff}) and λ_{S} (or S_{eff}) and the boundary conditions. If the effective advection and reaction work against the concentration gradient (so that the corresponding mass flux exceeds that given by effective diffusion), then the transport is diminished. This indicates that, to enhance the mass/heat transfer, the value of α and De should be carefully chosen, so that the effective advection and reaction assist in carrying the mass/heat from regions of high temperature or concentration to regions of low temperature or concentration.

In Fig. 6, we see that λ_{D}, λ_{U}, and λ_{S} increase with σ. However, this does not necessarily lead to the enhancement of effective mass/heat transfer because the effective advection and reaction might inhibit the transport if mass/heat is carried against the temperature or concentration gradient. Moreover, the increase in $\sigma = \hat{\mu}/\hat{\rho}\hat{D}$ requires a decrease in the molecular diffusivity $\hat{D}$ (for fixed $\hat{\mu}/\hat{\rho}$) or an increase in the kinematic viscosity $\hat{\nu} = \hat{\mu}/\hat{\rho}$ (for fixed $\hat{D}$), with the former generally reducing mixing, while the latter increasing the energy needed to drive the OSF. Note that Δr is a kinematic quantity independent of σ. Therefore, all the curves in Fig. 6(c) overlap.

2. Energy considerations for transport enhancement

We now consider the energy consumption associated with the OSF proposed herein for enhancing heat and/or mass transfer. To this end, in this section, we discuss the mass/heat flux, the consumed power to drive the upper plate, and the efficiency in a specific example.

Consider that a mass/heat source with a dimensionless radius of 0.1 is immersed in the center of an OSF device, as shown in Fig. 7. We assume that it has no influence on the local velocity field. This source ensures $\Lambda_0 = 1$ at $r = 0.1$. Suppose also that there is a mass/heat sink at $r = 1$, which

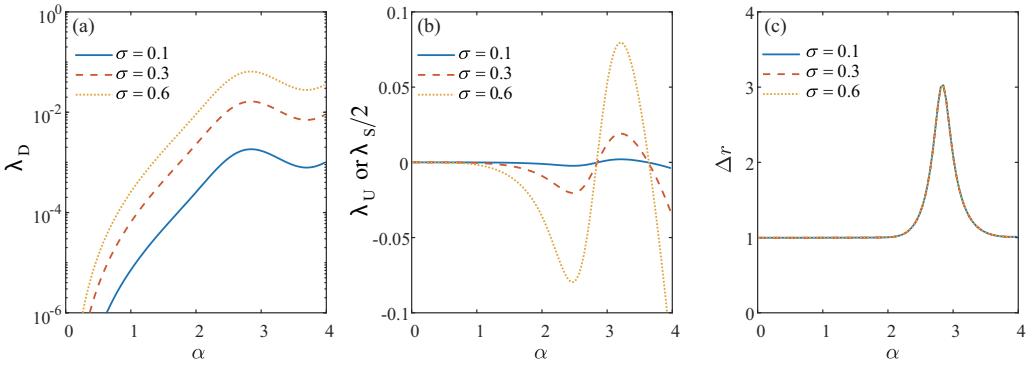

FIG. 6. The dependence of λ_D, λ_U (or $\lambda_S/2$), and Δr on α with different values of σ, at $r = 1$ when De $= 10$. The displacement of the upper plate satisfies $\delta = \epsilon$. The value of Pe is determined by $\mathrm{Pe} = \alpha^2\sigma\delta/\epsilon$. Note that $\lambda_U = \lambda_S/2$ for $r = 1$.

we assume not to affect the fluid flow but which forces $\Lambda_0 = 0$ at $r = 1$. The top and bottom plates are impermeable and insulated walls, thus the amount of mass/heat injected from the source must equal that absorbed by the sink at $r = 1$. With the boundary condition at $r = 1$, Eq. (27) is reduced into a diffusion equation, thus the mass/heat flux transported from the source to the sink can be calculated by

$$\dot{m}^* = -(1 + D_{\mathrm{eff}}) \left.\frac{\partial \Lambda_0}{\partial r}\right|_{r=1}. \tag{33}$$

The power required to drive the upper plate is found to be

$$\tilde{W}_T = \frac{1}{2\pi}\int_0^{2\pi} v|_{z=1}\tilde{F}_T \, \mathrm{d}t = -\mathrm{Re}\left\{\frac{i\pi f'''(1)}{16(1 + i\mathrm{De})}\right\}, \tag{34}$$

where $\tilde{F}_T$ is the excess normal force on the top plate (see Appendix C for details). We can then define a metric for the energy consumption per unit mass/heat flux, or efficiency,

$$\eta = \frac{\dot{m}^*}{\tilde{W}_T}. \tag{35}$$

The dependence of $\dot{m}^*$, $\tilde{W}_T$, and η on α, for a Maxwell fluid with De $= 30$, is shown in Fig. 8. For $\alpha < 1$, $\dot{m}^*$ is approximately constant (around 0.44) because $D_{\mathrm{eff}} \ll 1$ (see Fig. 4), indicating that the transport is mainly driven by molecular diffusion (or conduction), which is independent of α. For $\alpha > 1$, $\dot{m}^*$ oscillates about the value corresponding to molecular diffusion (or pure conduction). According to Eq. (33), $\dot{m}^*$ is influenced by both D_{eff} and $\partial\Lambda_0/\partial r$ at $r = 1$. The value of D_{eff} is

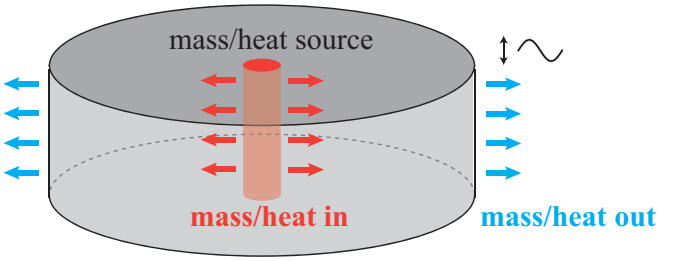

FIG. 7. An example of an OSF configuration for enhancing mass or heat transfer.

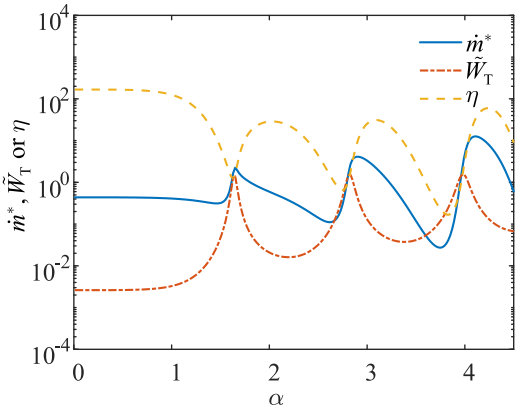

FIG. 8. The dependence of $\dot{m}^*$, η, and $\tilde{W}_T$ on α at steady state for a Maxwell fluid with $\mathrm{De} = 30$ and $\sigma = 0.6$. The amplitude of the oscillation of the upper plate is $\delta = 10\epsilon$. The value of Pe is determined by $\mathrm{Pe} = \alpha^2\sigma\delta/\epsilon$.

always positive and reaches a near-peak value at the resonant mode (see Fig. 4), indicating that the effective diffusion always enhances the mass or heat transfer, especially at resonance. However, the dependence of $\partial\Lambda_0/\partial r$ on α is more complex, as this strongly depends on U_{eff}, S_{eff}, and the boundary conditions.

In this example, when the values of U_{eff} and S_{eff} are positive, the value of $\partial\Lambda_0/\partial r$ is increased and thus the mass flux is enhanced; otherwise, the mass flux is diminished. For instance, the value of $\dot{m}^*$ is 30 times larger than that under pure molecular diffusion (which occurs when $\alpha \to 0$) when $\alpha \approx 4.1$, where both U_{eff} and S_{eff} are positive. On the other hand, the value of $\dot{m}^*$ is only 6% of that under pure molecular diffusion when $\alpha \approx 3.7$, because both U_{eff} and S_{eff} are negative and near the local minimum values. The value of $\tilde{W}_T$ rises as α is increased and reaches the local maximum exactly at the resonant mode, because the abrupt increase in velocity results in a significantly higher viscous loss. The efficiency η is large when $\alpha < 1$ because molecular diffusion (or pure conduction) does not consume energy; η drops when α approaches the first resonant frequency because of the increased $\tilde{W}_T$. In this example, we see that the mass/heat transfer in such OSF configurations strongly depends on the Womersley number α, which quantifies the oscillatory forcing of the flow. Thus, by choosing α suitably, we can either significantly increase the mass/heat flux and improve transport or decrease the flux of mass/heat transfer to a value even lower than that of the pure molecular diffusion or pure conduction.

IV. CONCLUSION

In this work, we have investigated Taylor-Aris dispersion related to mass and/or heat transfer in an oscillatory squeeze flow of a viscoelastic (Maxwell) fluid. First, we derived the expression for the posttransient velocity for both Newtonian and Maxwell fluids. Then we used the method of homogenization (a multiple-time-scale analysis) to determine the effective mass and/or heat transport equation on the long time scale. Specifically, we showed that transport is governed by an effective one-dimensional advection-diffusion-reaction equation. In doing so, we identified the three effective transport mechanisms: the effective diffusive spreading mass/heat along the concentration/temperature gradient, the effective advection carrying mass/heat along or against the concentration/temperature gradient, and the effective reaction releasing or absorbing mass/heat.

Importantly, we found resonances in the viscoleastic oscillatory squeeze flow, which lead to an abrupt rise in the velocity, when the Womersley number (a dimensionless measure of the forcing frequency and unsteady inertia of the fluid) reaches specific values. We showed that these resonant

values can be estimated by a simple expression involving the Deborah number. For a linearly viscoelastic Maxwell fluid, we found that there are multiple values of the Womersley number that may trigger the resonance, but the effect of resonance diminishes gradually with the Womersley number. We also observed that the mass/heat transfer in this viscoelastic fluid flow can be either enhanced or inhibited, depending on the value of the Womersley number. On the one hand, when the dimensionless frequency, i.e., the Womersley number, reaches the resonant frequency, the effective diffusion can be sharply enhanced, which accelerates the spread of mass/heat in the fluid. For instance, for a viscoelastic Maxwell fluid, we found that the effective diffusivity at the first resonant frequency can be 200 times larger than the corresponding one in the absence of a resonance. On the other hand, we found that the values of the effective advection and reaction coefficients oscillate about 0 with increasing amplitudes as the Womersley number increases. Notably, these two effective mechanisms may enhance or inhibit mass/heat transfer in this oscillatory viscoelastic flow, depending on their signs, which is determined by the Womersley number and the fluid properties (including the Deborah number and the Schmidt or Prandtl numbers). Therefore, to enhance the mass transfer, the value of the Womersley number should be carefully chosen, so that the effective advection and reaction help to carry solute from regions of high temperature or solute concentration to regions of low temperature or concentration.

The results presented in this work suggest a new approach to enhancing the mass/heat transfer using oscillatory squeeze flow. Further investigation could focus on the transport problem for high oscillation amplitudes, going beyond the assumptions inherent to the asymptotic nature of the homogenization theory employed here.

ACKNOWLEDGMENTS

This research was partially supported by Grant No. M2018/17 from the Israel Science Foundation (ISF). R.Y. was supported, in part, by a fellowship from the Israel Council for Higher Education. I.C.C. acknowledges the donors of the American Chemical Society Petroleum Research Fund for partial support under American Chemical Society Petroleum Research Fund Award No. 57371-DNI9. I.M.G. gratefully acknowledges support from the Royal Society through a University Research Fellowship. I.C.C., I.M.G., and G.Z.R. acknowledge the Collaborative Workshop Initiative for providing a platform to instigate this research, as well as H. A. Stone for many insightful discussions on Taylor dispersion.

APPENDIX A: DERIVATION OF THE EFFECTIVE ADVECTION-DIFFUSION-REACTION EQUATION USING THE HOMOGENIZATION METHOD

At $O(1)$, Eqs. (19) can be simplified as

$$\alpha^2\sigma\frac{\partial\Lambda_0}{\partial t_0}=\frac{\partial^2\Lambda_0}{\partial z^2}, \tag{A1a}$$

$$\left.\frac{\partial\Lambda_0}{\partial z}\right|_{z=0}=\left.\frac{\partial\Lambda_0}{\partial z}\right|_{z=h}=0. \tag{A1b}$$

If we seek the developed periodic solution, then Λ_0 is independent of the short time scale t_0. From system (A1) we find that Λ_0 is independent of z. Hence, $\Lambda_0=\Lambda_0(t_1,t_2,r)$.

At $O(\epsilon)$, Eq. (19) gives

$$\alpha^2\sigma\left(\frac{\partial\Lambda_0}{\partial t_1}+\frac{\partial\Lambda_1}{\partial t_0}\right)+\mathrm{Pe}\left[\frac{1}{r}\frac{\partial}{\partial r}(ru\Lambda_0)+\frac{\partial}{\partial z}(v\Lambda_0)\right]=\frac{\partial^2\Lambda_1}{\partial z^2}, \tag{A2a}$$

$$\left.\frac{\partial\Lambda_1}{\partial z}\right|_{z=0}=\left.\frac{\partial\Lambda_1}{\partial z}\right|_{z=h}=0. \tag{A2b}$$

Next, we introduce the temporal and spatial averaging operators

$$\overline{(\cdot)} = \frac{1}{2\pi}\int_t^{t+2\pi}(\cdot)\,\mathrm{d}t_0, \quad \langle\cdot\rangle = \frac{1}{h}\int_0^h(\cdot)\,\mathrm{d}z \simeq \int_0^1(\cdot)\,\mathrm{d}z. \tag{A3}$$

Note that $h \simeq 1$ since $\hat{a}/\hat{h}_0 \ll 1$. Time averaging Eqs. (A2a) and (A2b) gives

$$\alpha^2\sigma\frac{\partial\Lambda_0}{\partial t_1} = \frac{\partial^2\overline{\Lambda_1}}{\partial z^2}, \tag{A4a}$$

$$\left.\frac{\partial\overline{\Lambda_1}}{\partial z}\right|_{z=0} = \left.\frac{\partial\overline{\Lambda_1}}{\partial z}\right|_{z=h} = 0, \tag{A4b}$$

where we have used the fact that $\overline{u} = \overline{v} = 0$ because u and v are time-harmonic functions [see Eq. (12)] and $\overline{\Lambda_0} = \Lambda_0$ and $\langle\Lambda_0\rangle = \Lambda_0$ because Λ_0 is independent of t_0 and z, while $\overline{\partial\Lambda_1/\partial t_0} = 0$.

Applying spatial averaging to Eq. (A4a) [and from the related boundary conditions shown in Eq. (A4b)], we have

$$\frac{\partial\Lambda_0}{\partial t_1} = 0. \tag{A5}$$

With Eq. (A5), Eq. (A2a) can be simplified to

$$\alpha^2\sigma\frac{\partial\Lambda_1}{\partial t_0} + \mathrm{Pe}\left[\frac{1}{r}\frac{\partial}{\partial r}(ru\Lambda_0) + \frac{\partial}{\partial z}(v\Lambda_0)\right] = \frac{\partial^2\Lambda_1}{\partial z^2}. \tag{A6}$$

According to the simplification $\Lambda_0 = \Lambda_0(t_1, t_2, r)$ and Eq. (12), we have

$$\frac{\partial}{\partial z}(v\Lambda_0) = -\Lambda_0\mathrm{Re}\{f'(z)e^{it}\}, \tag{A7}$$

$$\frac{1}{r}\frac{\partial}{\partial r}(ru\Lambda_0) = \Lambda_0\mathrm{Re}\{f'(z)e^{it}\} + \frac{r}{2}\mathrm{Re}\{f'(z)e^{it}\}\frac{\partial\Lambda_0}{\partial r}. \tag{A8}$$

Substituting Eqs. (A7) and (A8) into Eq. (A6), we have

$$\alpha^2\sigma\frac{\partial\Lambda_1}{\partial t_0} + \mathrm{Pe}\,\mathrm{Re}\{f'(z)e^{it}\}\frac{r}{2}\frac{\partial\Lambda_0}{\partial r} = \frac{\partial^2\Lambda_1}{\partial z^2}, \tag{A9}$$

which indicates that the solution of Λ_1 is of the form

$$\Lambda_1 = r\frac{\partial\Lambda_0}{\partial r}\mathrm{Re}\{B_\mathrm{w}(z)e^{it}\}. \tag{A10}$$

Substituting Eq. (A10) into Eq. (A9), we have

$$\frac{\mathrm{d}^2B_w(z)}{\mathrm{d}z^2} - \frac{1}{2}\mathrm{Pe}f'(z) - i\alpha^2\sigma B_w(z) = 0, \tag{A11}$$

$$\left.\frac{\mathrm{d}B_w}{\mathrm{d}z}\right|_{z=0} = \left.\frac{\mathrm{d}B_w}{\mathrm{d}z}\right|_{z=h} = 0. \tag{A12}$$

At $O(\epsilon^2)$, Eqs. (19) give

$$\alpha^2\sigma\left(\frac{\partial\Lambda_2}{\partial t_0} + \frac{\partial\Lambda_1}{\partial t_1} + \frac{\partial\Lambda_0}{\partial t_2}\right) + \mathrm{Pe}\left[\frac{1}{r}\frac{\partial}{\partial r}(ru\Lambda_1) + \frac{\partial}{\partial z}(v\Lambda_1)\right] = \frac{1}{r}\frac{\partial}{\partial r}\left(r\frac{\partial\Lambda_0}{\partial r}\right) + \frac{\partial^2\Lambda_2}{\partial z^2}, \tag{A13a}$$

$$\left.\frac{\partial\Lambda_2}{\partial z}\right|_{z=0} = \left.\frac{\partial\Lambda_2}{\partial z}\right|_{z=h} = 0. \tag{A13b}$$

Equations (A10) and (A5) give

$$\frac{\partial \Lambda_1}{\partial t_1} = 0. \tag{A14}$$

Taking the cross-sectional average of Eq. (A13a), we have

$$\alpha^2\sigma\left(\frac{\partial\langle\Lambda_2\rangle}{\partial t_0} + \frac{\partial\Lambda_0}{\partial t_2}\right) + \mathrm{Pe}\left[\left\langle\frac{1}{r}\frac{\partial}{\partial r}(ru\Lambda_1)\right\rangle + (v\Lambda_1)\Big|_{z=0}^{z=1}\right] = \frac{1}{r}\frac{\partial}{\partial r}\left(r\frac{\partial\Lambda_0}{\partial r}\right) + \left\langle\frac{\partial^2\Lambda_2}{\partial z^2}\right\rangle. \tag{A15}$$

It can be shown that

$$\left\langle\frac{1}{r}\frac{\partial}{\partial r}(ru\Lambda_1)\right\rangle = \frac{\partial}{\partial r}\langle u\Lambda_1\rangle + \frac{1}{r}\langle u\Lambda_1\rangle, \tag{A16}$$

$$\left\langle\frac{\partial^2\Lambda_2}{\partial z^2}\right\rangle = \frac{\partial\Lambda_2}{\partial z}\Big|_{z=0}^{z=1} = 0; \tag{A17}$$

then Eq. (A15) can be written as

$$\alpha^2\sigma\left(\frac{\partial\langle\Lambda_2\rangle}{\partial t_0} + \frac{\partial\Lambda_0}{\partial t_2}\right) + \mathrm{Pe}\left[\frac{\partial}{\partial r}\langle u\Lambda_1\rangle + \frac{1}{r}\langle u\Lambda_1\rangle + (v\Lambda_1)\Big|_{z=0}^{z=1}\right] = \frac{1}{r}\frac{\partial}{\partial r}\left(r\frac{\partial\Lambda_0}{\partial r}\right). \tag{A18}$$

Taking the time average of Eq. (A18), we have

$$\alpha^2\sigma\frac{\partial\Lambda_0}{\partial t_2} + \mathrm{Pe}\left[\frac{\partial}{\partial r}\overline{\langle u\Lambda_1\rangle} + \frac{1}{r}\overline{\langle u\Lambda_1\rangle} + \overline{v\Lambda_1}\Big|_{z=0}^{z=1}\right] = \frac{1}{r}\frac{\partial}{\partial r}\left(r\frac{\partial\Lambda_0}{\partial r}\right). \tag{A19}$$

Additionally, from Eqs. (12) and (A10), we reach

$$\overline{\langle u\Lambda_1\rangle} = \frac{r^2}{4}\frac{\partial\Lambda_0}{\partial r}\mathrm{Re}\,\langle f'(z)^* B_{\mathrm{w}}(z)\rangle, \tag{A20}$$

$$\overline{v\Lambda_1}\Big|_{z=0}^{z=1} = -\frac{r}{2}\frac{\partial\Lambda_0}{\partial r}\mathrm{Re}\,\{iB_{\mathrm{w}}(1)\}. \tag{A21}$$

Substituting Eqs. (A20) and (A21) into Eq. (A19), we have

$$\alpha^2\sigma\frac{\partial\Lambda_0}{\partial t_2} = \frac{\partial^2\Lambda_0}{\partial r^2}\left[1 - \frac{r^2}{4}\mathrm{Re}\left\langle f'(z)^* B_{\mathrm{w}}(z)\right\rangle\mathrm{Pe}\right] + \frac{\partial\Lambda_0}{\partial r}\left[\frac{1}{r}\left(1 - \frac{r^2}{4}\mathrm{Re}\left\langle f'(z)^* B_{\mathrm{w}}(z)\right\rangle\mathrm{Pe}\right)\right.$$
$$\left. - \frac{r}{2}\mathrm{Re}\left\langle f'(z)^* B_{\mathrm{w}}(z)\right\rangle\mathrm{Pe} + \frac{r}{2}\mathrm{Re}\,\{iB_{\mathrm{w}}(1)\}\mathrm{Pe}\right]. \tag{A22}$$

Introducing the dimensionless effective diffusivity, velocity, and reaction terms shown in Eq. (26), Eq. (A22) can be arranged into Eq. (25).

APPENDIX B: DERIVATION OF THE COMPONENTWISE MOMENTUM EQUATIONS

The material derivative, assuming axisymmetry, is

$$\frac{\mathrm{D}}{\mathrm{D}\hat{t}} = \frac{\partial}{\partial\hat{t}} + \hat{u}\frac{\partial}{\partial\hat{r}} + \hat{v}\frac{\partial}{\partial\hat{z}}. \tag{B1}$$

Using the dimensionless variables from Eq. (8), we have

$$\frac{\mathrm{D}}{\mathrm{D}t} = \frac{\partial}{\partial t} + \delta u\frac{\partial}{\partial r} + \delta v\frac{\partial}{\partial z}. \tag{B2}$$

We recall that $\delta = \hat{a}/\hat{h}_0 \ll 1$ is the dimensionless displacement amplitude of the upper plate. Neglecting the small terms of $O(\delta)$, we obtain

$$\frac{\mathrm{D}}{\mathrm{D}\hat{t}} \simeq \frac{\partial}{\partial \hat{t}}. \tag{B3}$$

Next, combining Eq. (5) and Eq. (4) and acknowledging Eq. (B3), we have

$$\hat{\lambda}_0 \hat{\rho} \frac{\partial^2 \hat{\boldsymbol{u}}}{\partial \hat{t}^2} + \hat{\lambda}_0 \frac{\partial}{\partial \hat{t}} (\nabla \hat{p}) + \hat{\rho} \frac{\partial \hat{\boldsymbol{u}}}{\partial \hat{t}} = -\nabla \hat{p} + \hat{\mu} \nabla^2 \hat{\boldsymbol{u}}. \tag{B4}$$

From Eq. (B4), we obtain the componentwise momentum equations given in Eqs. (6a) and (6b).

APPENDIX C: ENERGY AND POWER REQUIREMENT

In the fully periodic regime, the dimensionless pressure is of the form

$$p = \mathrm{Re}\,\{p_0(r, z)e^{it}\}. \tag{C1}$$

Substituting Eqs. (12) and (C1) into Eq. (9a) at leading order in ϵ, we have

$$(1 + i\mathrm{De})\frac{\partial p_0}{\partial r} = (\mathrm{De} - i)\alpha^2 \frac{r}{2} f'(z) + \frac{r}{2} f'''(z). \tag{C2}$$

Integrating Eq. (C2), we obtain

$$p_0(r, z) = \frac{r^2}{4(1 + i\mathrm{De})}[(\mathrm{De} - i)\alpha^2 f'(z) + f'''(z)] + G(z), \tag{C3}$$

where $G(z)$ is an arbitrary function of integration. We define an *excess* pressure as

$$\tilde{p} = \mathrm{Re}\,\{\tilde{p}_0(r, z)e^{it}\}, \tag{C4}$$

where the amplitude $\tilde{p}_0$ is relative to the background pressure amplitude $p_0|_{r=1}$, i.e.,

$$\tilde{p}_0 = p_0 - p_0|_{r=1}. \tag{C5}$$

Substituting Eq. (C3) into Eq. (C5), we obtain

$$\tilde{p}_0(r, z) = \frac{r^2}{4(1 + i\mathrm{De})}[(\mathrm{De} - i)\alpha^2 f'(z) + f'''(z)] + G_2(z), \tag{C6}$$

where $G_2 = G - p_0|_{r=1}$. Solving for G_2 with the boundary condition of $\tilde{p}_0|_{r=1} = 0$, we obtain

$$\tilde{p}_0(r, z) = \frac{r^2 - 1}{4(1 + i\mathrm{De})}[(\mathrm{De} - i)\alpha^2 f'(z) + f'''(z)]. \tag{C7}$$

From Eq. (5), the componentwise equation for the stress tensor $\hat{\tau}_{zz}$ can be expressed as

$$\hat{\lambda}_0 \left(\frac{\partial \hat{\tau}_{zz}}{\partial \hat{t}} \right) = \hat{\mu}(\nabla \hat{v} + \nabla \hat{v}^T) - \hat{\tau}_{zz} = 2\hat{\mu} \frac{\partial \hat{v}}{\partial \hat{z}} - \hat{\tau}_{zz}. \tag{C8}$$

With the nondimensionalization in Eq. (8) and $\hat{\tau}_{zz} = \tau_{zz}\hat{\mu}\hat{a}\hat{\omega}/\epsilon^3\hat{R}$, we have

$$\frac{\mathrm{De}}{\epsilon^2} \frac{\partial \tau_{zz}}{\partial t} = 2\frac{\partial v}{\partial z} - \frac{1}{\epsilon^2}\tau_{zz}. \tag{C9}$$

By writing $\tau_{zz} = \mathrm{Re}\,\{\tau_{0,zz}(z)e^{it}\}$, we obtain

$$\tau_{zz} = -\mathrm{Re}\left\{ \frac{2\epsilon^2}{1 + i\mathrm{De}} f'(z)e^{it} \right\}. \tag{C10}$$

The scaled normal force on the top plate is found to be (see [28])

$$F_{\mathrm{T}} = 2\pi \int_0^1 \sigma_{zz}\, r\, \mathrm{d}r = 2\pi \int_0^1 (\tau_{zz} - p)|_{z=1} r\, \mathrm{d}r. \tag{C11}$$

Recalling that $f'(1) = 0$ from Eq. (14), Eq. (C11) can be simplified as

$$F_{\mathrm{T}} = -2\pi \int_0^1 p|_{z=1} r\, \mathrm{d}r. \tag{C12}$$

We define an excess normal force

$$\tilde{F}_{\mathrm{T}} = -2\pi \int_0^1 \tilde{p}|_{z=1} r\, \mathrm{d}r. \tag{C13}$$

Taking $\tilde{F}_{\mathrm{T}} = \mathrm{Re}\,\{\tilde{F}_{0,\mathrm{T}} e^{it}\}$ and substituting Eq. (C4) into Eq. (C13), we obtain

$$\tilde{F}_{0,\mathrm{T}} = \frac{\pi f'''(1)}{8(1 + i\mathrm{De})}. \tag{C14}$$

Hence, the power needed to drive the upper plate is

$$\tilde{W} = \frac{1}{2\pi} \int_0^{2\pi} v|_{z=1} \tilde{F}_T\, \mathrm{d}t = -\mathrm{Re}\left\{ \frac{i\pi f'''(1)}{16(1 + i\mathrm{De})} \right\}. \tag{C15}$$

[1] G. I. Taylor, Dispersion of soluble matter in solvent flowing slowly through a tube, Proc. R. Soc. London A **219**, 186 (1953).

[2] R. Aris, On the dispersion of a solute in pulsating flow through a tube, Proc. R. Soc. London A **259**, 370 (1960).

[3] R. Sankarasubramanian and W. N. Gill, Unsteady convective diffusion with interphase mass transfer, Proc. R. Soc. London A **333**, 115 (1973).

[4] T. Y. Lin and E. S. G. Shaqfeh, Taylor dispersion in the presence of cross flow and interfacial mass transfer, Phys. Rev. Fluids **4**, 034501 (2019).

[5] W. R. Young and S. Jones, Shear dispersion, Phys. Fluids A **3**, 1087 (1991).

[6] P. C. Chatwin, On the longitudinal dispersion of passive contaminant in oscillatory flows in tubes, J. Fluid Mech. **71**, 513 (1975).

[7] E. J. Watson, Diffusion in oscillatory pipe flow, J. Fluid Mech. **133**, 233 (1983).

[8] C. H. Joshi, R. D. Kamm, J. M. Drazen, and A. S. Slutsky, An experimental study of gas exchange in laminar oscillatory flow, J. Fluid Mech. **133**, 245 (1983).

[9] S. Vedel, E. Hovad, and H. Bruus, Time-dependent Taylor–Aris dispersion of an initial point concentration, J. Fluid Mech. **752**, 107 (2014).

[10] W. N. Gill and R. Sankarasubramanian, Dispersion of a non-uniform slug in time-dependent flow, Proc. R. Soc. London A **322**, 101 (1971).

[11] R. Smith, Contaminant dispersion in oscillatory flows, J. Fluid Mech. **114**, 379 (1982).

[12] F. Gentile, M. Ferrari, and P. Decuzzi, The transport of nanoparticles in blood vessels: The effect of vessel permeability and blood rheology, Ann. Biomed. Eng. **36**, 254 (2008).

[13] J. J. Fredberg, Augmented diffusion in the airways can support pulmonary gas exchange, J. Appl. Physiol. **49**, 232 (1980).

[14] D. M. Eckmann and J. B. Grotberg, Oscillatory flow and mass transport in a curved tube, J. Fluid Mech. **188**, 509 (1988).

[15] J. B. Grotberg, Pulmonary flow and transport phenomena, Annu. Rev. Fluid Mech. **26**, 529 (1994).

[16] L. Salerno, G. Cardillo, and C. Camporeale, Aris-Taylor dispersion in the subarachnoid space, Phys. Rev. Fluids **5**, 043102 (2020).

[17] S. M. Schmidt, M. J. McCready, and A. E. Ostafin, Effect of oscillating fluid shear on solute transport in cortical bone, J. Biomech. **38**, 2337 (2005).
[18] D. T. Leighton, Jr. and M. J. McCready, Shear enhanced transport in oscillatory liquid membranes, AIChE J. **34**, 1709 (1988).
[19] C. C. Mei and C. Chian, Dispersion of small suspended particles in a wave boundary layer, J. Phys. Oceanogr. **24**, 2479 (1994).
[20] G. Ramon, Y. Agnon, and C. Dosoretz, Solute dispersion in oscillating electro-osmotic flow with boundary mass exchange, Microfluid. Nanofluid. **10**, 97 (2011).
[21] G. Z. Ramon, Solute transport under oscillating electro-osmotic flow in a closed-ended cylindrical pore, J. Eng. Math. **110**, 195 (2018).
[22] U. H. Kurzweg and L. D. Zhao, Heat transfer by high-frequency oscillations: A new hydrodynamic technique for achieving large effective thermal conductivities, Phys. Fluids **27**, 2624 (1984).
[23] U. H. Kurzweg, Enhanced heat conduction in oscillating viscous flows within parallel-plate channels, J. Fluid Mech. **156**, 291 (1985).
[24] A. A. Lambert, S. Cuevas, J. A. del Río, and M. López de Haro, Heat transfer enhancement in oscillatory flows of Newtonian and viscoelastic fluids, Int. J. Heat Mass Transf. **52**, 5472 (2009).
[25] R. Li, W. Mu, T. Sun, X. Li, and X. Wang, Benchmark study of a small-scale slab track system with squeeze-mode magnetorheological fluid isolators, J. Intell. Mater. Syst. Struct. **29**, 52 (2018).
[26] S. L. Wingstrand, N. J. Alvarez, O. Hassager, and J. M. Dealy, Oscillatory squeeze flow for the study of linear viscoelastic behavior, J. Rheol. **60**, 407 (2016).
[27] N. Phan-Thien, Small strain oscillatory squeeze film flow of simple fluids, J. Aust. Math. Soc. Ser. B, Appl. Math. **22**, 22 (1980).
[28] N. Phan-Thien and R. I. Tanner, Viscoelastic squeeze-film flows—Maxwell fluids, J. Fluid Mech. **129**, 265 (1983).
[29] J. S. Field, M. V. Swain, and N. Phan-Thien, An experimental investigation of the use of random squeezing to determine the complex modulus of viscoelastic fluids, J. Non-Newton. Fluid Mech. **65**, 177 (1996).
[30] J. Engmann, C. Servais, and A. S. Burbidge, Squeeze flow theory and applications to rheometry: A review, J. Non-Newton. Fluid Mech. **132**, 1 (2005).
[31] D. Bell, D. M. Binding, and K. Walters, The oscillatory squeeze flow rheometer: Comprehensive theory and a new experimental facility, Rheol. Acta **46**, 111 (2006).
[32] H. A. Stone and H. Brenner, Dispersion in flows with streamwise variations of mean velocity: Radial flow, Ind. Eng. Chem. Res. **38**, 851 (1999).
[33] J. L. Creech, A. Chauhan, and C. J. Radke, Dispersive mixing in the posterior tear film under a soft contact lens, Ind. Eng. Chem. Res. **40**, 3015 (2001).
[34] J. R. Womersley, Method for the calculation of velocity, rate of flow and viscous drag in arteries when the pressure gradient is known, J. Physiol. **127**, 553 (1955).
[35] J. Kevorkian and J. D. Cole, Multiple Scale and Singular Perturbation Methods, *Applied Mathematical Sciences*, Vol. 114 (Springer-Verlag, New York, 1996).
[36] C. C. Mei and B. Vernescu, *Homogenization Methods for Multiscale Mechanics* (World Scientific, Singapore, 2010).
[37] C. O. Ng, Dispersion in steady and oscillatory flows through a tube with reversible and irreversible wall reactions, Proc. R. Soc. London A **462**, 481 (2006).
[38] M. Pagitsas, A. Nadim, and H. Brenner, Multiple time scale analysis of macrotransport processes, Physica A **135**, 533 (1986).
[39] P. C. Fife and K. R. K. Nicholes, Dispersion in flow through small tubes, Proc. R. Soc. London A **344**, 131 (1975).
[40] C. C. Mei, J. L. Auriault, and C. O. Ng, Some applications of the homogenization theory, Adv. Appl. Mech. **32**, 277 (1996).
[41] H. C. W. Chu, S. Garoff, T. M. Przybycien, R. D. Tilton, and A. S. Khair, Dispersion in steady and time-oscillatory two-dimensional flows through a parallel-plate channel, Phys. Fluids **31**, 022007 (2019).

[42] J. R. Womersley, *An Elastic Tube Theory of Pulse Transmission and Oscillatory Flow in Mammalian Arteries*, Tech. Rep. WADC TR 56-614 (Aerospace Research Labs, Wright-Patterson Air Force Base, OH, 1957).

[43] C. Loudon and A. Tordesillas, The use of the dimensionless Womersley number to characterize the unsteady nature of internal flow, J. Theor. Biol. **191**, 63 (1998).

[44] J. R. Castrejón-Pita, J. A. del Río, A. A. Castrejón-Pita, and G. Huelsz, Experimental observation of dramatic differences in the dynamic response of Newtonian and Maxwellian fluids, Phys. Rev. E **68**, 046301 (2003).

[45] U. H. Kurzweg and M. J. Jaeger, Tuning effect in enhanced gas dispersion under oscillatory conditions, Phys. Fluids **29**, 1324 (1986).